



# Dielectric relaxation in $\text{CaMnO}_3$ ceramics synthesized by sol–gel method

K. R. Nandan<sup>1,\*</sup>, Laurel Simon Lobo<sup>2</sup>, G. Murugesan<sup>3</sup>, N. Maruthi<sup>1</sup>, and A. Ruban Kumar<sup>4</sup>

<sup>1</sup>Department of Physics, Faculty of Engineering and Technology, Jain Deemed to be University, Bangalore 562112, India

<sup>2</sup>Center for Regional Revitalization in Research and Education, Department of Material Science and Engineering, Akita University, 1-1 Tegatagakuen-cho, Akita 010-8502, Japan

<sup>3</sup>Department of Physics, Vel Tech Rangarajan Dr.Sagunthala R & D Institute of Science and Technology, Chennai 600062, India

<sup>4</sup>Centre for Crystal Growth, School of Advanced Sciences, Vellore Institute of Technology, Vellore, India

Received: 26 February 2021

Accepted: 12 May 2021

Published online:

2 June 2021

© The Author(s), under exclusive licence to Springer Science+Business Media, LLC, part of Springer Nature 2021

## ABSTRACT

Calcium manganites ( $\text{CaMnO}_3$ ) ceramic powders were prepared by sol–gel technique using citric acid as a chelating agent. The polycrystalline powder crystallized in an orthorhombic structure with lattice parameters  $a = 5.270 \text{ \AA}$ ,  $b = 7.421 \text{ \AA}$  and  $c = 5.231 \text{ \AA}$ . Dielectric relaxation was observed which can be attributed to Maxwell–Wagner relaxation behavior. The oxidation states of Calcium, Manganese and the presence of oxygen deficiencies in the prepared samples were ascertained by XPS studies.

## 1 Introduction

Perovskite structured materials have gain attraction in technological point of view in various fields of sensors, microwave absorbers, pigments, catalysts, magnetic storage and microelectronics [1]. Perovskite oxides like  $\text{ATiO}_3$  (A=Ca, Sr) ceramics are promising n-type thermoelectric materials due to the flexibility of doping on both the sites [2]. The  $\text{AMnO}_3$  (A=Ca, La, Sr, Ba) crystal structure consists of corner sharing octahedral where Mn is surrounded by six oxygen atoms with A locating the cavities [3]. The structure of  $\text{AMnO}_3$  ceramics makes it feasible for doping of several dopants to tailor its properties [4, 5]. Among

them  $\text{CaMnO}_3$  have gained special attention due to their peculiar structural, thermoelectric, magnetic and electrical properties [3]. Calcium manganite crystallizes in an orthorhombic structure with n-type semiconductor characteristics [6]. The flexibility in the crystal structure of  $\text{CaMnO}_3$  makes it more feasible for several dopants on both the sites to alter its properties [5]. Calcium manganites possess high thermal conductivity, high Seebeck coefficient and appreciable electrical conductivity [5]. The variation of oxygen content in calcium manganites over a broad range makes it a potential candidate as cathode in solid oxide fuel cells [7].  $\text{CaMnO}_3$  possess superior thermoelectric properties like high Seebeck

Address correspondence to E-mail: nandan88.kr@gmail.com

coefficient and low values of electrical conductivity which makes it a promising material for thermo-electric applications [6]. Several synthesis techniques like solid-state reaction [8], chemical coprecipitation method [9], electrostatic spray deposition [10], gas phase reaction synthesis [11], soft chemistry synthesis [12] were adapted to prepare  $\text{CaMnO}_3$  ceramics. Herein we have synthesized  $\text{CaMnO}_3$  by sol-gel technique to achieve a homogeneous sample with uniform particle size, morphology and high crystallinity. The dielectric behavior of  $\text{CaMnO}_3$  have not been extensively analyzed; this thrived our interest to carryout dielectric measurements at higher temperatures and herein we report about the dielectric relaxation present in the prepared  $\text{CaMnO}_3$  sample.

## 2 Experimental methods

Adopting sol-gel technique  $\text{CaMnO}_3$  ceramics have been prepared using citric acid as a chelating agent. The initial precursors Calcium nitrate ( $\text{Ca}(\text{NO}_3)_2 \cdot 4\text{H}_2\text{O}$ ), and Manganese nitrate ( $\text{Mn}(\text{NO}_3)_2 \cdot 4\text{H}_2\text{O}$ ) are taken in stoichiometric ratios and dissolved in deionized water to obtain the homogenous solution. Citric acid solution ( $\text{C}_6\text{H}_8\text{O}_7$ ) is added drop wise to the homogenous solution and stirred continuously for about 3 h in room temperature. Later the solution is heated up to  $80^\circ\text{C}$  and stirred well until the formation of gel. The obtained gel is dried in a vacuum oven at  $120^\circ\text{C}$ . Further it was pre-sintered at  $300^\circ\text{C}$  in air for 4 h to remove the organic constituents present in it. The final product is obtained after sintering it at  $800^\circ\text{C}$  for 5 h and it is ground into fine powders for further characterizations.

## 3 Results and discussion

### 3.1 X-ray diffraction studies

The crystallinity and phase formation of the synthesized material were found by measuring the X-ray diffraction patterns in a  $2\theta$  range from  $10^\circ$  to  $80^\circ$  using Bruker D8 advance (Cu  $\text{K}\alpha$  radiation,  $\lambda = 1.5406 \text{ \AA}$ ). The powder diffraction patterns of  $\text{CaMnO}_3$  polycrystalline material calcined at  $800^\circ\text{C}$  is shown in Fig. 1. The diffraction patterns revealed that the synthesized material crystallized in an orthorhombic structure (space group  $\text{Pnma}$ ) without

any secondary phases. The lattice parameters of the crystalline material were found to be  $a = 5.270 \text{ \AA}$ ,  $b = 7.421 \text{ \AA}$ ,  $c = 5.231 \text{ \AA}$  and volume found to be  $204.577 \text{ \AA}^3$ .

### 3.2 Dielectric studies

The  $\text{CaMnO}_3$  powder is made into pellets and coated by silver paste for carrying out electrical measurements. The dielectric measurements were carried out in the frequency range 50 Hz to 5 MHz at various temperatures using a LCR meter (HIOKI3532-50LCR meter HITESTER). The variation of dielectric constant with frequency for various temperature ranges are shown in Fig. 2. On increasing the temperature the dielectric constant value increases due to the thermal activation of charge carriers [13]. Due to the presence of space charge polarization and grain boundary effect, the dielectric constant increases at lower frequency regions [14]. At higher temperatures the dielectric constant increases due to the rise of conduction in the prepared sample.

### 3.3 Impedance studies

The frequency dependence of real part of impedance ( $Z'$ ) for increasing temperatures are shown in Fig. 3. At lower frequency region, the values of  $Z'$  seems to be constant for all the temperatures due to the accumulation of charge carriers at the electrode interface and grain boundaries. On increasing the frequency and temperature,  $Z'$  values decrease due to the

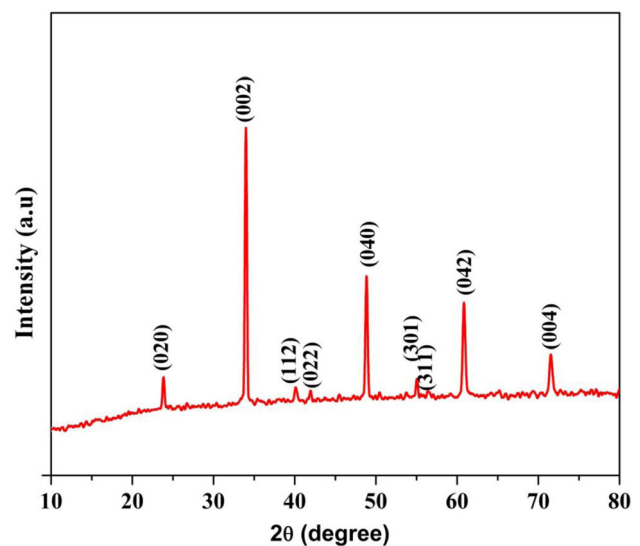


Fig. 1 XRD pattern of  $\text{CaMnO}_3$  sample

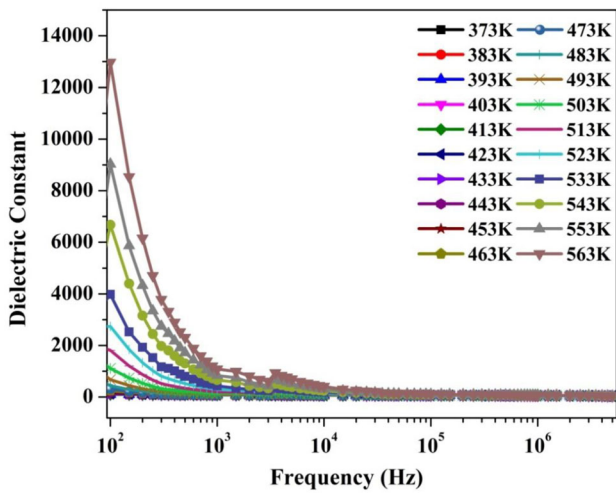


Fig. 2 Variation of dielectric constant with frequency for different temperature of CaMnO<sub>3</sub>

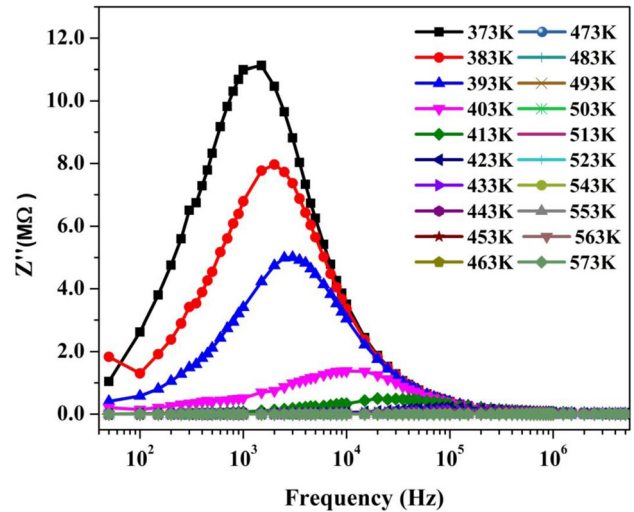


Fig. 4 Variation of Z'' with frequency for different temperatures

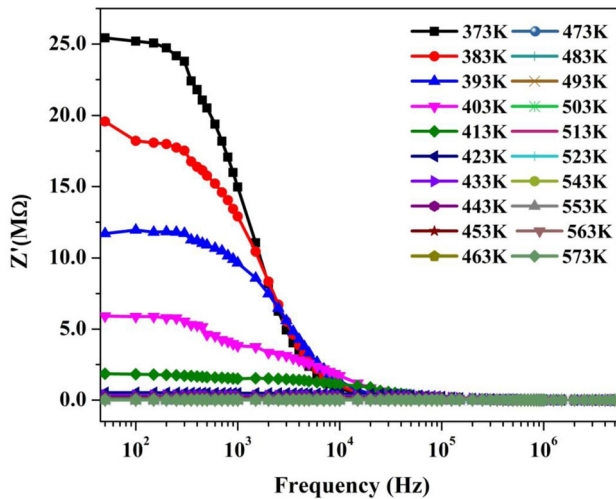


Fig. 3 Variation of Z' with frequency for different temperatures

enhancement of conductivity in the prepared material. This phenomena attributes to the behavior of negative temperature coefficient of resistance that usually occurs in semiconducting materials [15, 16].

The frequency dependence of imaginary part of impedance (Z'') for increasing temperatures is shown in Fig. 4. On increasing the temperature, a peak shift is observed toward the higher frequency side which indicates the spreading of relaxation in the material. On increasing the temperature, the Z'' values decrease signifying the existence of thermally activated charge carriers. The presence of temperature-dependent relaxation in the prepared samples were validated by the broadening of peaks [17]. At higher

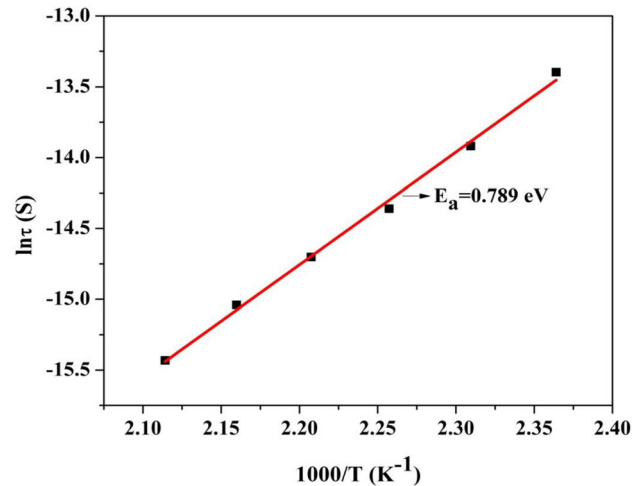
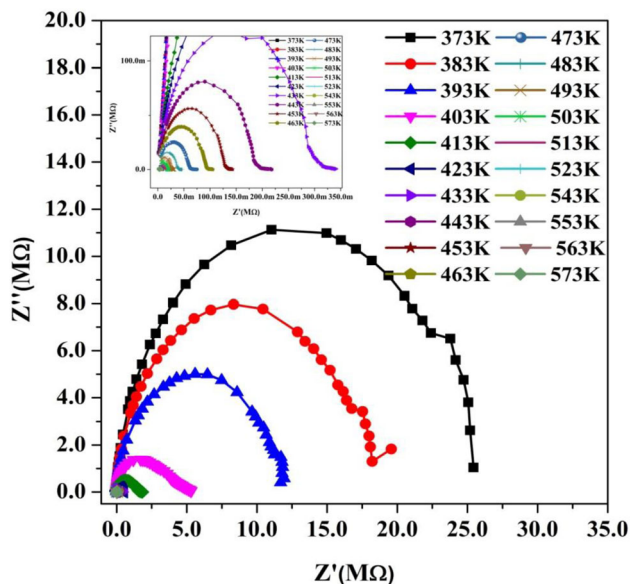


Fig. 5 Arrhenius plot of temperature dependence of relaxation time from variation of imaginary part of impedance with frequency

frequencies the accumulation of charges in the electrode interface results in the merging of Z'' [14]. The high-temperature synthesis of oxide ceramics results in the presence of oxygen vacancies which contributes the relaxation phenomenon in the prepared material.

The variation of relaxation time for different temperatures (Arrhenius plot) is shown in Fig. 5, the activation energy is found to be 0.789 eV. The value of activation energy signifies the origin of dielectric relaxation is due to the presence of oxygen vacancies [16].



**Fig. 6** Nyquist plots of impedance data for different temperatures of  $\text{CaMnO}_3$

To analyze the contribution of grain, grain boundary and interfacial effects separately, Nyquist plots for various temperatures are plotted (Fig. 6). On increasing the temperature, depression in the center of semicircle is observed due to the presence of thermally activated conduction process [18].

At lower temperatures, single semicircle is observed which is attributed to the grain conduction mechanism and on increasing the temperature the grain effect is dominated by grain boundary effect. The presence of a semicircle at lower frequencies (Inset of Fig. 6) denotes the existence of space charge polarization effect. From the plot it can be observed

that the grain resistance decreases for increasing temperature and the irregular semicircles at higher temperatures may be due to grain boundary stress-strain, grain size distribution, volume fraction and defects in the material [13]. The presence of dielectric relaxations in the prepared samples have resulted in the occurrence of depressed semicircles. Complete semicircles were not observed due to the dominance of electrode polarization effect at lower frequency regions [19]. The frequency dependence of ac conductivity for different temperatures is fitted by Jonscher's Power law (Fig. 7a). Deviation was observed from the fitting for the lower frequency regions due to domination of electrode polarization effect. The activation energy for obtained from the Arrhenius fit (Fig. 7b) is found to be 0.898 eV. The activation energy value attributes to the oxygen vacancies, localized ions and hopping of electrons present in the material [20, 21].

### 3.4 XPS studies

The oxidation state of the Calcium, Manganese and presence of oxygen vacancies was confirmed by carrying out XPS studies. The XPS survey spectra (Fig. 8a) for the synthesized  $\text{CaMnO}_3$  ceramics reveal the presence of Ca, Mn, O and C without any other impurity peak. The two Mn 2p peaks (Fig. 8b) corresponding to  $\text{Mn}2\text{P}_{3/2}$  and  $\text{Mn}2\text{P}_{1/2}$  are centered around 643 eV and 655 eV, respectively. Both the peaks seem to be asymmetric and contains an additional peak which corresponds to the presence of  $\text{Mn}^{4+}$ , this confirms the presence of oxygen vacancies

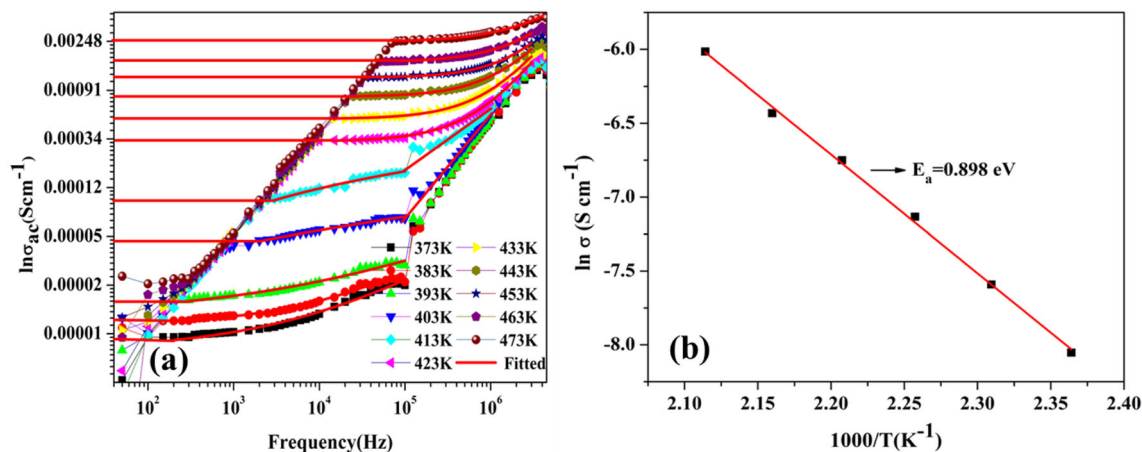
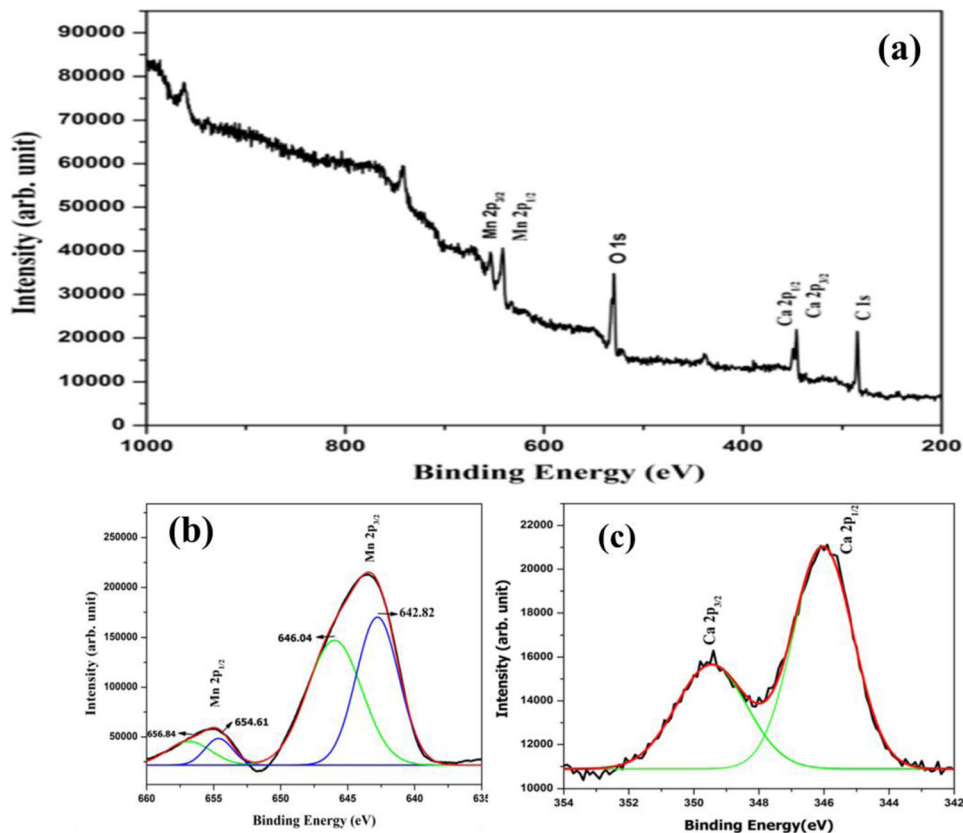


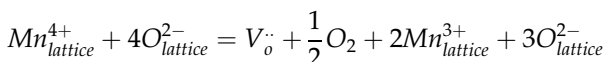
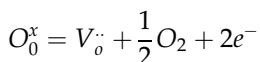
**Fig. 7** **a** Variation of frequency versus  $\sigma_{ac}$  conductivity fitted with Jonscher power Law for different temperature. **b** Arrhenius behavior of dc conductivity  $\ln(\sigma)$  versus  $1000/T$  from frequency-dependent conductivity for different temperature



**Fig. 8** XPS Spectra of synthesized CaMnO<sub>3</sub> **a** survey spectra and high resolution, **b** Mn 2p, **c** Ca 2p



in the prepared samples [22]. The reduction of Mn<sup>4+</sup> to Mn<sup>3+</sup> ions are related to the oxygen vacancies present due to the oxygen vacancies as a consequence of high-temperature sintering. The charge neutrality is maintained by the following mechanism [23]:



The XPS spectra for Ca2p are shown in Fig. 8c, the peak centered around 346 eV and 349.5 eV corresponds to Ca2P<sub>1/2</sub> and Ca2P<sub>3/2</sub>, respectively [24].

### 4 Conclusions

Ceramic powders of CaMnO<sub>3</sub> were synthesized by sol–gel technique using citric acid as chelating agent. The synthesized material crystallized to an orthorhombic structure. Maxwell–Wagner relaxation were observed in the dielectric measurements for temperature ranges between 373 and 573 K. The presence of electrode polarization effect was

observed in the Nyquist plot and in conductivity measurements. The existence of Mn<sup>3+</sup> and Mn<sup>4+</sup> states for manganese is confirmed by XPS studies which clearly evident the presence of oxygen vacancies in the prepared samples.

### References

1. T. Herranz, S. Rojas, M. Ojeda, F.J. Pérez-Alonso, P. Terreros, K. Pirota, J.L.G. Fierro, Synthesis, structural features, and reactivity of Fe–Mn mixed oxides prepared by microemulsion. *Chem. Mater.* **18**(9), 2364–2375 (2006)
2. J.W. Fergus, Oxide materials for high temperature thermoelectric energy conversion. *J. Eur. Ceram. Soc.* **32**(3), 525–540 (2012)
3. F.P. Zhang, X. Zhang, Q.M. Lu, J.X. Zhang, Y.Q. Liu, Electronic structure and thermal properties of doped CaMnO<sub>3</sub> systems. *J. Alloys Compd.* **509**(10), 4171–4175 (2011)
4. W.S. Tan, H.P. Wu, K.M. Deng, X.S. Wu, Q.J. Jia, J. Gao, Studies on strain relaxation and in-plane orientation of La<sub>0.7</sub>Ca<sub>0.3</sub>MnO<sub>3</sub> film by grazing incidence X-ray diffraction. *J. Alloys Compd.* **491**(1–2), 545–549 (2010)

5. D.H. Manh, P.T. Phong, T.D. Thanh, L.V. Hong, N.X. Phuc,  $\text{La}_{0.7}\text{Ca}_{0.3}\text{MnO}_3$  perovskite synthesized by reactive milling method: the effect of particle size on the magnetic and electrical properties. *J. Alloys Compd.* **491**(1–2), 8–12 (2010)
6. S.D.O. Torres, D. Thomazini, G.P. Balthazar, M.V. Gelfuso, Microstructural influence on thermoelectric properties of  $\text{CaMnO}_3$  ceramics. *Mater. Res.* (2020). <https://doi.org/10.1590/1980-5373-mr-2020-0169>
7. M. Schrade, R. Kabir, S. Li, T. Norby, T.G. Finstad, High temperature transport properties of thermoelectric  $\text{CaMnO}_{3-\delta}$ —indication of strongly interacting small polarons. *J. Appl. Phys.* **115**(10), 103705 (2014)
8. N. Pandey, A.K. Thakur, R.N.P. Choudhary, *Studies on Dielectric Behaviour of an Oxygen Ion Conducting Ceramic—CaMnO<sub>3-δ</sub>* (CSIR, Chennai, 2008).
9. J. Lan, Y.H. Lin, H. Fang, A. Mei, C.W. Nan, Y. Liu et al., High-temperature thermoelectric behaviors of fine-grained Gd-doped  $\text{CaMnO}_3$  ceramics. *J. Am. Ceram. Soc.* **93**(8), 2121–2124 (2010)
10. K. Fujimoto, M. Gibu, Y. Yamaguchi, A. Aimi, K. Nishio, O. Rabin, I. Takeuchi, Thermoelectric properties of bismuth-substituted calcium manganite  $\text{Ca}_{1-x}\text{Bi}_x\text{MnO}_{3-\delta}$  prepared via the electrostatic spray deposition method. *J. Ceram. Soc. Jpn.* **125**(4), 308–312 (2017)
11. K. Koumoto, Y. Wang, R. Zhang, A. Kosuga, R. Funahashi, Oxide thermoelectric materials: a nanostructuring approach. *Annu. Rev. Mater. Sci.* **40**, 363–394 (2010)
12. L. Bocher, M.H. Aguirre, R. Robert, D. Logvinovich, S. Bakardjieva, J. Hejtmanek, A. Weidenkaff, High-temperature stability, structure and thermoelectric properties of  $\text{CaMn}_{1-x}\text{Nb}_x\text{O}_3$  phases. *Acta Mater.* **57**(19), 5667–5680 (2009)
13. L.S. Lobo, S. Kalainathan, A.R. Kumar, Investigation of electrical studies of spinel  $\text{FeCo}_2\text{O}_4$  synthesized by sol–gel method. *Superlattices Microstruct.* **88**, 116–126 (2015)
14. K.R. Nandan, A.R. Kumar, Electrical properties of  $\text{Ca}_{0.925}\text{Ce}_{0.075}\text{Mn}_{1-x}\text{Fe}_x\text{O}_3$  ( $x = 0.1\text{--}0.3$ ) prepared by sol–gel technique. *J. Mater. Sci. Mater. Electron.* **27**(12), 13179–13191 (2016)
15. N. Kumari, V. Kumar, S.K. Singh, Structural, dielectric and magnetic investigations on  $\text{Al}^{3+}$  substituted Zn-ferrospinel. *RSC Adv.* **5**(47), 37925–37934 (2015). <https://doi.org/10.1039/C5RA03745J>
16. L.S. Lobo, A.R. Kumar, Investigation of structural and electrical properties of  $\text{ZnMn}_2\text{O}_4$  synthesized by sol–gel method. *J. Mater. Sci. Mater. Electron.* **27**(7), 7398–7406 (2016). <https://doi.org/10.1007/s10854-016-4714-z>
17. L.S. Lobo, A.R. Kumar, Structural and electrical properties of  $\text{ZnCo}_2\text{O}_4$  spinel synthesized by sol–gel combustion method. *J. Non-Cryst. Solids* **505**, 301–309 (2019). <https://doi.org/10.1063/1.4794349>
18. S.G. Mohamed, C.J. Chen, C.K. Chen, S.F. Hu, R.S. Liu, High-performance lithium-ion battery and symmetric supercapacitors based on  $\text{FeCo}_2\text{O}_4$  nanoflakes electrodes. *ACS Appl. Mater. Interfaces* **6**(24), 22701–22708 (2014). <https://doi.org/10.1021/am5068244>
19. G. Murugesan, R. Nithya, S. Kalainathan, Colossal dielectric behaviour of  $\text{Sr}_2\text{TiMnO}_{6-\delta}$  single crystals. *J. Cryst. Growth* **530**, 125179 (2020)
20. L.S. Lobo, A.R. Kumar, Investigation on structural and electrical properties of  $\text{FeMnO}_3$  synthesized by sol–gel method. *Ionics* **25**(3), 1341–1350 (2019). <https://doi.org/10.1007/s11581-018-2776-z>
21. S. Yuvaraj, V.D. Nithya, K.S. Fathima, C. Sanjeeviraja, G.K. Selvan, S. Arumugam, R.K. Selvan, Investigations on the temperature dependent electrical and magnetic properties of  $\text{NiTiO}_3$  by molten salt synthesis. *Mater. Res. Bull.* **48**(3), 1110–1116 (2013). <https://doi.org/10.1016/j.materresbull.2012.12.001>
22. B. Zhang, A. Chang, Q. Zhao, H. Ye, Y. Wu, Synthesis and thermoelectric properties of Yb-doped  $\text{Ca}_{0.9-x}\text{Yb}_x\text{La}_{0.1}\text{MnO}_3$  ceramics. *J. Electron. Mater.* **43**(11), 4048–4055 (2014)
23. S. Jaiswar, K.D. Mandal, Evidence of enhanced oxygen vacancy defects inducing ferromagnetism in multiferroic  $\text{CaMn}_7\text{O}_{12}$  manganite with sintering time. *J. Phys. Chem. C* **121**(36), 19586–19601 (2017)
24. L. He, G. Dong, C. Deng, Effects of strontium substitution on the phase transformation and crystal structure of calcium phosphate derived by chemical precipitation. *Ceram. Int.* **42**(10), 11918–11923 (2016)

**Publisher's Note** Springer Nature remains neutral with regard to jurisdictional claims in published maps and institutional affiliations.